Nano Today 34 (2020) 100900

Contents lists available at ScienceDirect

Nano Today

journal homepage: www.elsevier.com/locate/nanotoday

Ultralong and efficient phosphorescence from silica confined carbon nanodots in aqueous solution

Ya-Chuan Liang[a], Shan-Shan Gou[b], Kai-Kai Liu[a,*], Wen-Jie Wu[a], Chen-Zi Guo[c], Si-Yu Lu[d], Jin-Hao Zang[a], Xue-Ying Wu[a], Qing Lou[a], Lin Dong[a], Yan-Feng Gao[b,*], Chong-Xin Shan[a,*]

[a] Henan Key Laboratory of Diamond Optoelectronic Materials and Devices, Key Laboratory of Material Physics, Ministry of Education, School of Physics and Microelectronics, Zhengzhou University, Zhengzhou 450001, China
[b] School of Life Sciences, Zhengzhou University, Zhengzhou 450001, China
[c] Changchun Institute of Optics, Fine Mechanics and Physics, Chinese Academy of Sciences, Changchun 130033, China
[d] College of Chemistry and Molecular Engineering, Zhengzhou University, 100 Kexue Road, Zhengzhou 450001, China

ARTICLE INFO

Article history:
Received 23 February 2020
Received in revised form 6 May 2020
Accepted 20 May 2020

Keywords:
Water-soluble
Carbon nanodots
Phosphorescence
Afterglow imaging

ABSTRACT

Water-soluble phosphorescent nanoparticles are highly desirable for biomedical applications. However, the phosphorescence of nanoparticles is usually quenched in aqueous solutions due to the nonradiative deactivation of triplet excitons by the oxygen in water, thus it is a huge challenge to realize water-soluble phosphorescent nanoparticles. Herein, ultralong and efficient phosphorescence has been achieved from water-soluble carbon nanodots (CNDs) by confine CNDs in a nanospace. Silica capsulation layer is used to ensure the solublity of the CNDs, isolate the CNDs from the surrounding oxygen in the aqueous solution. Furthermore, the motion and vibration of covalent bonds in the CNDs are limited. In this way, the nonradiative deactivation rates of triplet excitons has been decreased, and efficient phosphorescence is achieved from water-soluble CNDs. The lifetime and phosphorescence quantum yield of the CNDs are 1.86 s and 11.6 %, both of which are the best values ever reported for water-soluble phosphorescent nanoparticles. In terms of the efficient phosphorescence of the CNDs in aqueous solution, *in vivo/vitro* afterglow imaging is also been demonstrated.

Luminescent nanomaterials including quantum dots, dyes and rare-based up-conversation nanoparticles used as optical agents have been used for *in vivo*/*vitro* bioimaging [1–3]. However, the external excitation light is needed during the imaging process, which can cause the autofluorescence of tissue. Room phosphorescent nanomaterials with long-lasting luminescence after cessations of illumination source can address this issue because it can permit bioimaging without real-time external light, which are of great interest in the field of optoelectronic devices [4], bioimaging, [5,6] biotherapy [7] and information security [8,9]. Generally, the way to achieve room temperature phosphorescence (RTP) can be mainly divided into two categories: One route is to enhance the spin-orbit coupling (SOC) by the introduction of hetero atoms (*e.g.*, N, P, and halogens) or aromatic carbonyl groups to promote the intersystem crossing (ISC) efficiency [10–13]. The other route is to restrict molecule vibration and rotation with the assistance of matrix or crystal to stabilize the triplet excitons [14–17]. To date, efficient phosphorescence are mainly limited to metal-coordination based materials and organic compounds [18–22]. As for metal-coordination based RTP materials, they usually suffered from high cost, cytotoxicity, and complicated preparation process [23–25]. While the triplet excitons of organic compounds are easy to relax *via* nonradiative decay due to vibration and rotation of covalent bonds. More importantly, most of the reported phosphorescent materials are in solid form, and phosphorescence will be quenched in water ambient, which hinders the application of phosphorescent nanomaterials in bioimaging greatly. Therefore, it is highly desirable to develop water-soluble RTP nanoparticles with good biocompatibility and ultralong lifetime.

As a newly emerged luminescent nanomaterial, carbon nanodots (CNDs) have aroused enormous attention thanks to their unique optical properties [26–33], facile preparation and good biocompatibility, which have been widely used in bioimaging and biotherapy [34–36]. In addition to fluorescence, the RTP of CNDs has been achieved by fastening CNDs into a variety of matrices such

* Corresponding authors.
E-mail addresses: liukaikai@zzu.edu.cn (K.-K. Liu), gaoyf@zzu.edu.cn (Y.-F. Gao), cxshan@zzu.edu.cn (C.-X. Shan).

https://doi.org/10.1016/j.nantod.2020.100900
1748-0132/

as polyvinyl alcohol [37], recrystallized urea/biuret [16], potassium aluminum sulfate [38] and zeolites [39]. These matrices can effectively restrict the vibration and rotation of CNDs, thus prevent the triplet states of CNDs from nonradiative decay processes. Unsurprisingly, all the above mentioned RTP of CNDs were achieved in solid matrix [17], and it is still a huge challenge to realize water-soluble CNDs to date [40,41]. Recently, the incorporation of CNDs and melamine or SiO_2 were used to achieve RTP in aqueous solution but they are still confronted with short emission lifetimes or poor phosphorescence efficiency, which hindered their application in biological field [42,43]. The phosphorescence lifetime and efficiency of the CNDs is determined by the radiative transition and nonradiative transition rates, and the radiative transition rates are much smaller than that of nonradiative transition. As for the phosphorescence of the CNDs in water, the nonradiative transition mainly through the following two paths: vibration/rotation and dissolved oxygen. Thus efficient phosphorescence from water-soluble CNDs can be achieved if the mentioned issues are addressed.

In our previous work, enhanced phosphorescence and fluorescence of organic microrods and quantum dots in water solution have been demonstrated, providing a valuable inspiration [44,45]. Herein, water-soluble phosphorescent CNDs (WSP-CNDs @ silica) have been prepared by confining the CNDs in a silica encapsulation layer, and the phosphorescence lifetime and quantum yield (QY) of the phosphorescence can reach 1.86 s and 11.6 %, both of which are the best values ever reported for water-soluble phosphorescent nanoparticles. The mechanism for the long lifetime and efficient phosphorescence can be attributed to the confinement of the silica shell outside the CNDs that restricts the rotation and vibration of the bonds in the CNDs. Furthermore, the silica shell can also isolate the CNDs from dissolved oxygen in aqueous solution, thus help to reduce the nonradiative rates of the water-soluble CNDs. As a result, ultralong and efficient phosphorescence has been observed from the CNDs in aqueous solution. The water-soluble phosphorescent CNDs show high stability, good biocompatibility, which is favorable for afterglow bioimaging. In *vivo/vitro* afterglow imaging has been demonstrated based on the WSP-CNDs @ silica, which promises applications of CNDs in the field of afterglow bioimaging.

Results and disscussion

The processes that occur between the absorption and emission of CNDs are depicted by a simplified Jablonski diagram, as shown in Fig. 1(a). Following excitation, CNDs is excited form ground state S_0 to higher singlet state (S_1 or S_2, only S_1 is presented for simplication). The CNDs in S_1 state undergo a ISC process to the first triplet T_1. The phosphorescence transition rates (K_p) are about 10^3 s^{-1} or smaller, whereas the nonradiative transition rates (k_{nr1} and k_{nr2}) are in the range of 10^9 s^{-1}. By definition, the lifetime and phosphorescence quantum yield can be calculated by the following equation:

$$\tau_p = 1/(k_p+k_{nr1}+k_{nr2})$$

$$QY = k_p/(k_p+k_{nr1}+k_{nr2})$$

Where τ_p is lifetime, QY is phosphorescence quantum yield. Usually, the triplet excitons of CNDs in water are depopulated through nonradiative pathway, as shown in the left of Fig. 1(a). If the CNDs are confined in a nanospace, the k_{nr1} and k_{nr2} will be reduced greatly, and the ultralong and efficient phosphorescence from water-soluble CNDs is expected to achieve.

Hetero atom doping in CNDs can facilitate ISC and lead to effectively populate triplet excitons, ethylenediamine (EDA) and phosphoric acid (PA) were selected as the raw materials to product CNDs. Subsequently, dialysis and freeze-drying were conducted to remove unreacted raw materials and phosphorescent CND powder was obtained. As a proof-of-concept, silica is used as nanospace to confine the CNDs in terms of its good bio-compatibility. CNDs aqueous solution is premixed with ammonia and tetraethoxysilane (TEOs) and then the above solution stirred for 8 h at room temperature, as illustrated in Fig. 1(b). Covalent bonds between silica and the CNDs were constructed to restrict and insulate CNDs in order to achieve phosphorescence in aqueous solution. Through restriction and insulation effect of the outside silica, the triplet states of the CNDs were stable and the triplet-to-triplet transition between the CNDs and oxygen ($^3O_2$) was forbidden, thus the ultralong phosphorescence of the water-soluble CNDs was achieved, as shown in Fig. 1(b). In view of their good water solubility, biocompatibility and ultralong lifetime, the attempt in *vivo/vitro* afterglow imaging has been performed. This work will stimulate the research on water-soluble phosphorescent CNDs due to their great applications prospects in afterglow bioimaging.

The CNDs with different lifetimes can be achieved through control the extent of carbonization, and the lifetimes of CNDs synthesized at different carbonization times are shown in Fig. S1 and the optimal carbonization time is 130 s. For convenience, three CNDs have been chosen for discussion. The images of the three CNDs with UV on and UV off are shown in Fig. 2(a). The corresponding lifetime decay curves of the CNDs were recorded, as shown in Fig. S2. The as-prepared CNDs with short, moderate and long lifetime are denoted as CND-1, CND-2 and CND-3, respectively. The morphologies and the structure of the CND-1, CND-2 and CND-3 were characterized by transmission electron microscope (TEM). The TEM images of CND-1, CND-2 and CND-3 are shown in Fig. 2(b), (c) and (d), respectively. All of the CNDs display quasi-spherical shape with diameter of about 4 nm. No obvious lattice fringes can be observed in CND-1 (Inset of Fig. 2(b)), demonstrating the polymeric structure. The high-resolution TEM images of CND-2 and CND-3 illustrate the lattice spacing of 0.21 nm which corresponds to the d-spacing of the graphene (100) planes, as shown inset of Fig. 2(c) and (d). The full width at half maxima of the three CNDs in XRD spectra decreases with the increase of carbonization time, suggesting the extent of crystallization increases gradually with increase of carbonization time (Fig. S3(a)). The XRD result of the three CNDs is consistent with the result of TEM. The ratio of I_G/I_D (intensity of G band/D band) is characteristic of the extents of sp^2/sp^3 carbon, the typical Raman spectra of the three CNDs were recorded, as shown in Fig. S3(b). Two peaks at 1320 cm^{-1} and 1561 cm^{-1} correspond to the disordered (D band) and graphite (G band) carbon. The ratio of I_D/I_G is 1.06, 0.986, and 0.95 for CND-1, CND-2, and CND-3, respectively. The decrease ratio value implies that more ordered carbon cores were formed in the CND-3, leading to a stable structure and triplet states are thus stabilized in turn. The survey X-ray photoelectron spectroscope (XPS) spectra (Fig. S4) of the three CNDs reveal that all of the CNDs contain C (284.6 eV), N (401.0 eV), O (531.8 eV), and P (133.0 eV and 190.0 eV) elements. The N and P elements in the CNDs were in favor of ISC due to hetero atom doping in CNDs can enhance spin-orbit coupling.

The photophysical properties of the three CNDs are investigated as shown in Figs. 2(e)–(g) and S5. The transparent solution of the three CNDs shows strong fluorescence but there is no phosphorescence. The UV–vis absorption spectra of the three CNDs are shown in Fig. S5. The UV–vis absorption spectra of the three CNDs exhibit a strong absorption peak at around 350 nm, which can be assigned to the n-π^* transition. The photoluminence (PL) excitation spectra of the three CNDs are close to the absorption band at 350 nm, indicating that the emission is originated from the n-π^* transition. Notably, the presence of C=N groups can facilitate the ISC according to the reported literature. The phosphorescence spectra of the CND-2 and CND-3 powder exhibit strong phosphorescence with a peak centered at around 520 nm (Fig. S6). The CND-3 with

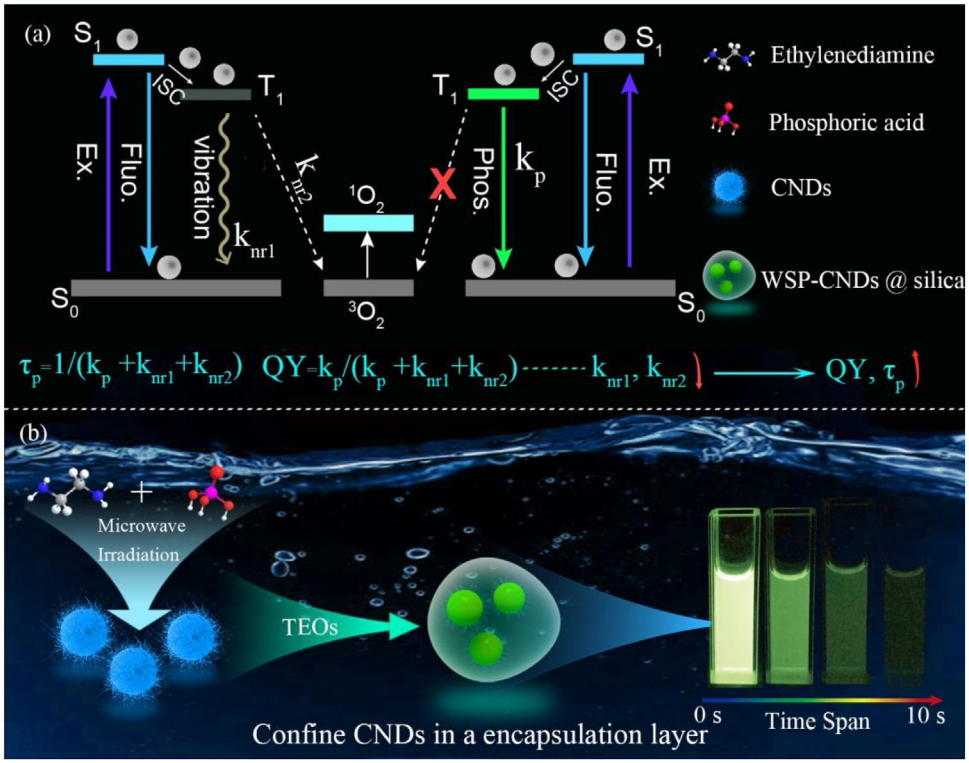

Fig. 1. Proposed possible phosphorescence mechanism of CNDs in aqueous solution (a) and schematic illustration of the preparation process (b) of the WSP- CNDs @ silica.

long lifetime was taken as an example, and the phosphorescence excitation-emission contour of the CND-3 was shown in Fig. 2e. The PL excitation wavelength located in the range from 330 nm to 360 nm, and the optimum excitation wavelength located at in the 350 nm. The lifetimes of CND-3 in powder and aqueous solution were 1.33 s and 1.99 ns (Figs. S1(c) and S7), indicating the phosphorescence emission can only be achieved in solid form. The temperature dependent transient decay curves of the CND-3 were recorded from 78 to 353 K, as shown in Fig. 2(f). The lifetime decreases with the rising of temperature, and this is characteristic property of phosphorescence materials. A small energy difference between S_1 and T_1 (ΔE_{ST}) is favor of the population of triplet excitons. The ΔE_{ST} of CNDs can be estimated through their low temperature fluorescence and phosphorescence spectra. In Figs. 2(g) and S8, low temperature fluorescence and phosphorescence spectrum of the CND-3 at 77 K show two emission peaks at 448 nm and 505 nm and the $\Delta E_{ST} = E_S - E_T$ = 1240/448 eV – 1240/505 eV = 0.31 eV. The time-resolved emission spectra (TRES) revealed the ultralong phosphorescence emission of CND-3 (Fig. 2(h)) and the lifetime of CND-3 raised to 1.33 s under the excitation of 350 nm. A possible internal structure of as-prepared CND-3 has been proposed based on above results, as shown in Fig. 2(i), and phosphorescence emission mechanism of the CND-3 was further discussed. EDA can react with phosphoric acid and further form covalently-crosslinked frameworks, which can suppress the nonradiative transitions effectively. In addition, hydrogen bonds in CND-3 can further decrease vibration and rotation, thus restricting the rotation motion of the CND-3. N atoms with lone pair electrons are favor of the production of the triplet excitons through n-π^* transition, which can facilitate the spin-forbidden transition from singlet to triplet states. The n-π^* transition mainly occurs between two repeated units C=N. Taken together, the strong interaction between luminescent units of the CND-3 play a key role in the ultralong phosphorescence. In Fig. 2(j), a possible transition model was proposed: N atoms with lone pair electrons promote electrons transition from single state to triplet state. The strong interaction (Hydrogen bond) between luminescent units of the CND-3 stabilizes the triplet electrons. Thus, the electrons can populate the triplet state effectively, and then the electrons will go back to S_0 state from T_1 with phosphorescence emission.

To endow the CND-3 good water-soluble property as well as ultralong lifetime, the CND-3 should be capsuled into hydrophilic nano-silica, as illustrated in Fig. S9. The optimal preparation conditions of the water-soluble phosphorescent CNDs are investigated from three aspects (Tetraethyl orthosilicate (TEOs) concentration, preparation time and the CND-3 concentration), as shown in Fig. S10. The fluorescence and phosphorescence intensities of the water-soluble phosphorescent CNDs with different TEOs are shown in Fig. S10(a). The fluorescence and phosphorescence intensity of the water-soluble phosphorescent CNDs reaches a maximum when the TEOs volume was 0.5 mL. The phosphorescence intensity of the water-soluble phosphorescent CNDs gradually increases and then almost keeps as the increase of the time of hydrolysis and the optimal hydrolysis time is 8 h. (Fig. S10(b)). The volume of the CND-3 also influences the fluorescence and phosphorescence intensity, and the optimal concentration of the CNDs is 1 mL (100 μg/mL), as shown in Fig. S10(c). As a result, the optimal preparation condition for the water-soluble phosphorescent CNDs is 1 mL (100 μg/mL) CND-3 aqueous solution and 0.5 mL tetraethoxysilane (TEOs) were dispersed in 15 mL deionized water (DI) to form aqueous solution. Then, 0.5 mL ammonia was added into the above solution stirring for 8 h at room temperature. The possible chemical reactions between TEOs and CNDs have been reported before, which are discussed as follows [46]: The gelation process of silica can be described by two types of reactions, generally referred to the hydrolysis and subsequent condensation reaction. In Fig. S11, TEOs can be hydrolyzed by water to form intermediate product 1 (IP1) (reaction 1), and then the hydroxyl groups onto the surface of CNDs can react with TEOs according to reaction 2. Finally, the CNDs are encapsulated in silica to form WSP-CNDs @ silica. The morphol-

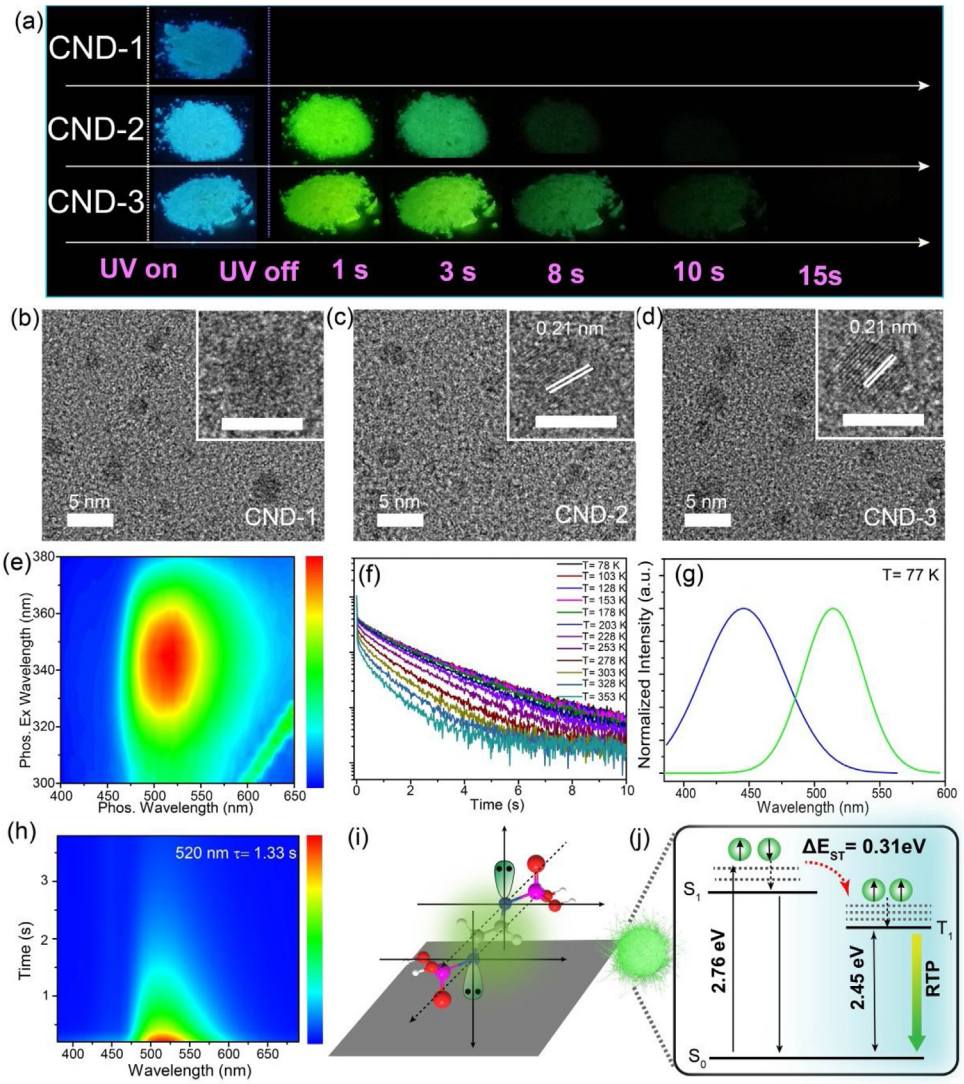

Fig. 2. (a) The photographs of the CND-1, CND-2, and CND-3 (powder) with UV on and UV off. TEM images of CND-1 (b), CND-2 (c), and CND-3 (d), the insets are high-resolution TEM images. (Scale bar: 5 nm). (e) Phosphorescence excitation-emission contour for the CND-3. (f) Temperature-dependent transient decay curves of the CND-3. (g) Deconvolution of the low temperature (77 K) fluorescence (blue curve) and phosphorescence (green curve) spectra of CND-3 under excitation at 365 nm. (h) Time-resolved emission spectra of the CND-3. (i) The single luminescence unit of the CND-3. (j) Proposed mechanism for ultralong phosphorescence of CND-3.

ogy and structure of the water-soluble phosphorescent CNDs were characterized by TEM, as shown in Fig. 3(a). From the TEM image, one can see that the nanoparticles are coated with amorphous silica shell, which meets our mentioned design requirement. As a result, the CND-3 are restricted in a nanospace and this will restrict their vibration, rotation and insulate of oxygen, achieving ultralong water soluble phosphorescent CNDs. The FTIR spectra (Fig. 3b) of the water-soluble phosphorescent CNDs display the presence of Si-OH (3454 cm^{-1}) and Si-O-Si (1089 cm^{-1}) stretching vibrations, indicating the CND-3 have been coated by silica. In addition, the characteristic vibration centered at 890 cm^{-1} and 1456 cm^{-1} came from N-Si and C-Si bonds, respectively, indicating that covalent bonds between the CND-3 and external silica have formed. The full XPS spectrum (Fig. 3c) of the water-soluble phosphorescent CNDs demonstrates that the water-soluble phosphorescent CNDs mainly contain C, N, O, P and Si elements. The high resolution XPS spectra of C 1s, N 1s, P 1s and Si 1s were measured, as shown in Fig. S12. The C-N/C=N (285.4 eV), C-C/C=C (284.6 eV), C-O (285.4 eV) bonds can be observed in C 1s spectrum. The N 1s spectrum reveals the presence of N-Si (398 eV) and amino N (399 eV). The P 1s spectrum contains two peaks at 131.9 eV and 130.9 eV for P=N and P-O bonds. The Si 2p spectrum can be deconvoluted into two peaks at 100.4 eV and 101.4 eV for Si-O and C-Si bonds. The above results suggest that the CND-3 and silica have combined through covalent bond, and covalent bonds can limit the vibration of the CND-3, which can promote their phosphorescence in aqueous solution. The fluorescence and phosphorescence spectra of the water-soluble phosphorescent CNDs are shown in Fig. 3(d) and the inset is the fluorescence and phosphorescence image. The absorption spectra of the water-soluble phosphorescent CNDs exhibit two absorption peaks (Fig. S13) at around 280 and 350 nm, which may derive from the π-π* and n-π* transitions of C-C/C=C and C=N. Moreover, in view of the good consistency between their excitation and absorption spectra, the n-π* transition may be responsible for their fluorescence and phosphorescence emission. The water-soluble phosphorescent CNDs exhibit a peak centered at around 520 nm with an excitation wavelength of 350 nm (Figs. 3d and S14), which is consistent with the CND-3 powder. The lifetime decay curve of the water-soluble phosphorescent CNDs collected at 520 nm is shown in Fig. 3(e), and the corresponding lifetime is 1.86 s, which is the longest lifetime of water soluble nanoparticles ever reported. Compared with the CND-3 powder, water-soluble phosphorescent CNDs are confined

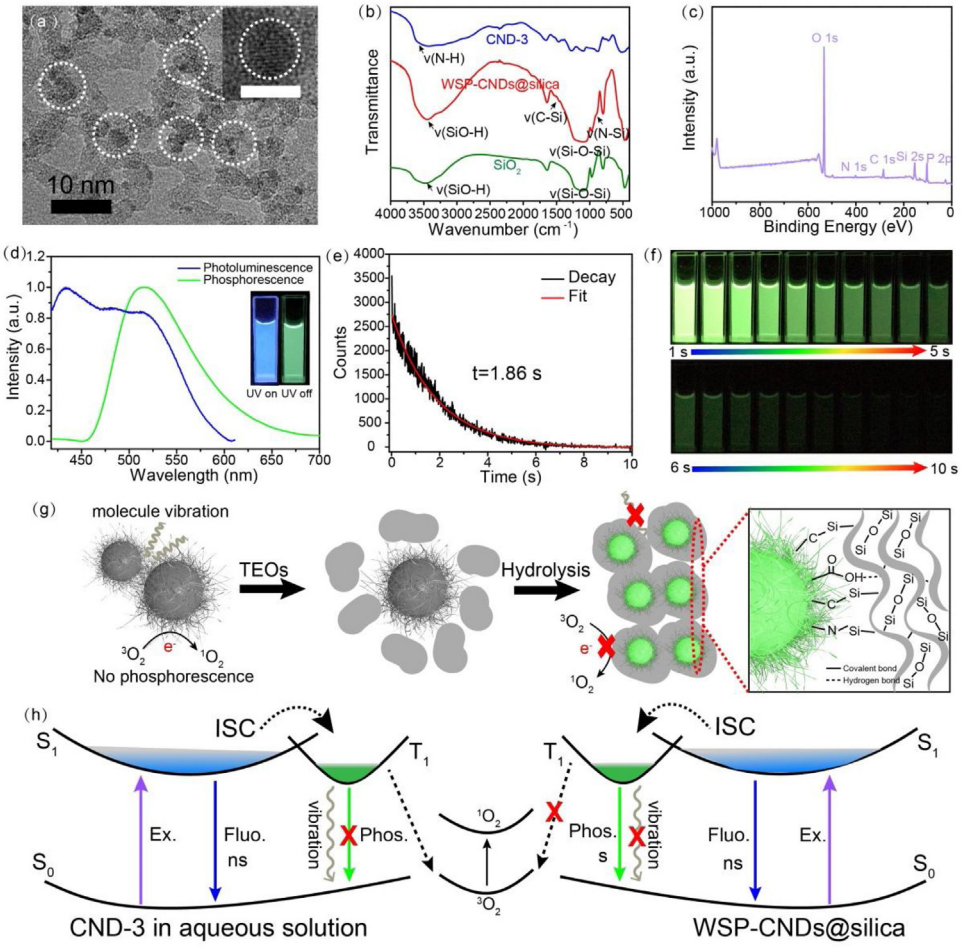

Fig. 3. (a) TEM image of WSP-CNDs @ silica (Inset is the magnified image of WSP-CNDs @ silica). (b) FTIR spectra of the CND-3, WSP-CNDs @ silica and prepared silica. (c) XPS spectrum of the WSP-CNDs @ silica. (d) The fluorescence and phosphorescence spectra of the WSP-CNDs @ silica. (e) Lifetime decay curve of the WSP-CNDs @ silica collected at 520 nm. (f) The images of the WSP-CNDs @ silica after UV irradiation. (g) Phosphorescence mechanism of the as-prepared WSP-CNDs @ silica. (h) Proposed mechanism for ultralong phosphorescence of the WSP-CNDs @ silica.

Table 1
Summarized reported work about water-soluble phosphorescent nanoparticles.

Reference	Materials	Phosphorescence lifetime (s)	Phosphorescence QY (%)
[42]	M-CDs	0.269	×
[43]	CDs@SiO_2	1.64	×
[41]	CD-CA	0.687	×
[5]	OSN1-T	0.861	1.59
[47]	C-C4-Br	0.14	11
[48]	*m*-PBCM	0.71	10.2
This work	WSP-CNDs @ silica	1.86	11.6

in a silica encapsulation layer, and the rotation and vibration of the bonds in the CNDs are restricted. Furthermore, the silica shell can also isolate the CNDs from surrounding oxygen, thus help to reduce the nonradiative rates. Thus, the lifetime of WSP-CNDs @ silica in water is longer than that of CND-3 powder without the capsulation of silica layer. The quantum yield (QY) of the phosphorescence in aqueous solution can reach 11.6 %, which are the best values ever reported for water-soluble phosphorescent nanoparticles. The reported works about water-soluble phosphorescent nanoparticles are summarized, and the corresponding phosphorescence lifetimes and quantum yields are shown in Table 1. The phosphorescence radiative (k_p) and nonradiative (k_{nr}) transition rates are calculated as shown in Table S1. The k_p of the WSP-CNDs @ silica is 0.062 s^{-1} and the k_{nr} is 0.475 s^{-1}. It can be found that the nonradiative transition rate of the WSP-CNDs @ silica is very slow due to the confinement effect of silica matrix, which can make WSP-CNDs @ silica ultralong phosphorescence in aqueous solution. In addition, bright green phosphorescence of the WSP-CNDs @ silica can be easily observed by the naked eye for nearly 10 s after removing UV irradiation, as shown in Fig. 3f. The corresponding luminescence video of the WSP-CNDs @ silica in aqueous solution is shown in Video S1. The effects of oxygen are studied using the singlet oxygen sensor green (SOSG) as a detector, which can emit green fluorescence when they meet with singlet oxygen. The CND-3 and WSP-CNDs @ silica are mixed with SOSG solution respectively, and then the fluorescence intensities are recorded after illumination. For the CND-3 group, the SOSG fluorescence intensity exhibits a great enhancement after illumination for 2 mins (Fig. S15, green line), which indicates that CND-3 can generate singlet oxygen due to the reaction with surrounding triplet oxygen. For the WSP-CNDs @ silica group, the fluorescence intensity of the SOSG is far lower than that of in CND-3 group, as shown in Fig. S15. This result indicates that the WSP-CNDs @ silica can isolate surrounding oxygen and block intramolecular electron transfer between WSP-CNDs @ silica and oxygen. A possible mechanism and the corresponding energy level diagrams for the WSP-CNDs @ silica are illustrated in Fig. 3(g) and (h). The phosphorescence of the CND-3 will be quenched due to the molecule rotation and vibration; on the other hand the triplet states transition between the CND-3 and dissolved oxygen is easy to occur. Thus, silica was used to isolate the CND-

3 with surrounding oxygen in order to achieve phosphorescence in aqueous solution. The covalent bonds between silica and the CND-3 can efficiently limit molecular rotation and vibration, thus the ultralong phosphorescence of the water-soluble CNDs can be achieved.

The stability of the water-soluble phosphorescent CNDs was assessed in view of the practical applications. The temporal stability of the water-soluble phosphorescent CNDs is a key issue that determines the performance when they are used in living organism, thus the temporal stability of the water-soluble phosphorescent CNDs was analyzed (Fig. S16). The phosphorescence intensity of the water-soluble phosphorescent CNDs keeps almost unchanged within 40 days and the aqueous solution maintains clear and transparent without any precipitation, indicating the good stability of the water-soluble phosphorescent CNDs synthesized in this route. The photo stability of the water-soluble phosphorescent CNDs was also accessed, as shown in Fig. S17. The phosphorescence intensity of the water-soluble phosphorescent CNDs can maintain constant after UV illumination for 35 min, and it can be activated repeatedly with no obvious decrease in phosphorescence intensity aspect, indicating the good photo stability of the water-soluble phosphorescent CNDs. Additionally, the phosphorescence intensity of the water-soluble phosphorescent CNDs under nitrogen and oxygen atmosphere is shown in Fig. S18, reflecting their immunity to oxygen. Moreover, phosphorescence intensity can keep constant even in NaCl aqueous solution with high concentration (Fig. S19), which this is key issue in view of biological application.

MTT assays were performed to evaluate the cytotoxicity of the WSP-CNDs @ silica before biological applications. The cell viability of the CHO-K1 cells decrease weakly even when the concentration of the WSP-CNDs @ silica increase to 100 μg/mL and cell viabilities are above 90 % after incubating 48 h, as shown in Fig. 4(a). Additionally, there is no significant difference in proliferation of the cells in presence of the WSP-CNDs @ silica. The morphology and density of the cells do not show any significant differences after incubating with the WSP-CNDs @ silica for 24, 48 and 72 h, as shown in Fig. S20. In order to evaluate the cytotoxicity of the WSP-CNDs @ silica further, CCK-8 experiment was performed using Hela, Lo2 and Hu7 cells as indicated in Fig. S21. There is a slight decline in the cell viability of the three kinds of cells even when the concentration of the WSP-CNDs @ silica is up to 100 μg/mL, indicating the relatively low biological toxicity of the WSP-CNDs @ silica. The low biological toxicity of the WSP-CNDs @ silica indicated that they can be used in biological applications. To evaluate the potential applications of the WSP-CNDs @ silica in bioimaging, flow cytometry assays were conducted to quantify the binding efficiency of the WSP-CNDs @ silica to DC2.4 cells, as shown in Fig. 4(b). The cells incubated with the WSP-CNDs @ silica exhibited stronger phosphorescence than that of the control group, 2.6-fold enhancement was determined by flow cytometry analysis (Fig. 4(c)). For bioimaging, the DC2.4 cells were incubated with the WSP-CNDs @ silica (100 μg/mL) for 2 h and then washed with PBS buffer, their luminescence images were recorded on a confocal microscope. The bright-field images of the DC2.4 cells are shown in Fig. 4(d1) and (e1). Fig. 4(d2) shows the fluorescence image of the DC2.4 cells under 405 nm illumination. Blue emission signal of the cells can be detected in the range from 408 nm to 500 nm, indicating the WSP-CNDs @ silica are distributed into cytoplasm of the DC2.4 cells uniformly. The merged images of

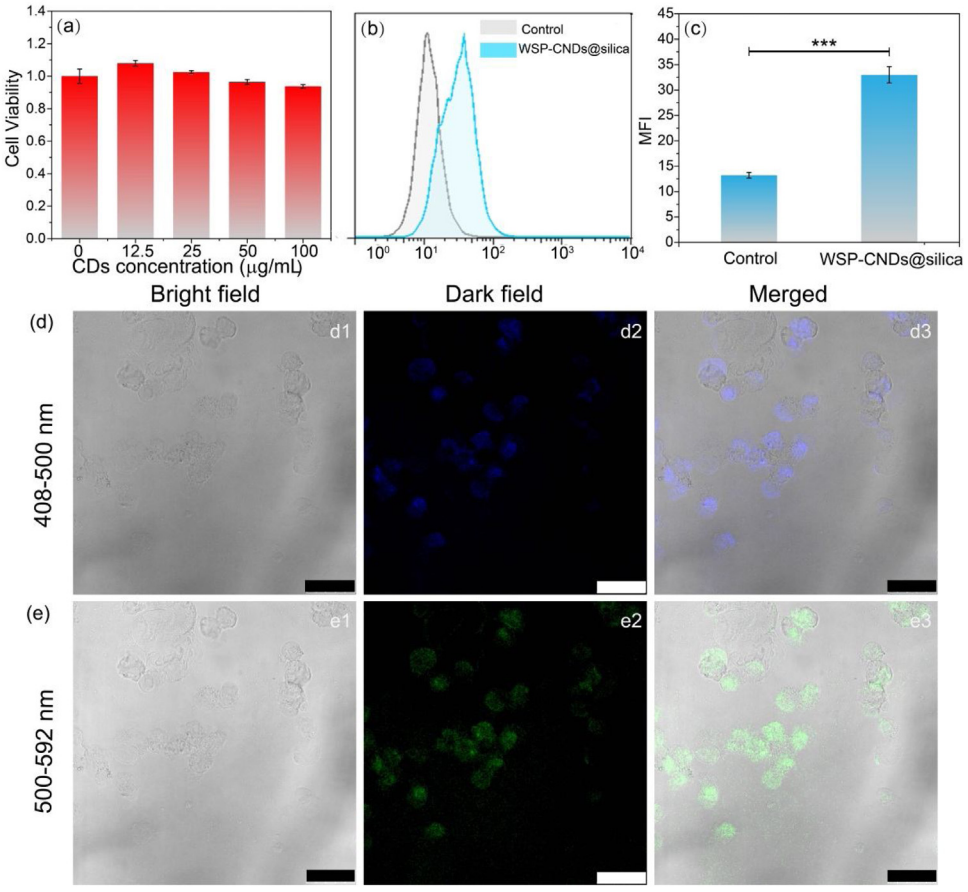

Fig. 4. (a) The cytotoxicity assay of the WSP-CNDs @ silica. (b) Flow cytometer analysis of the WSP-CNDs @ silica (100 μg/mL) after UV illumination. (c) Statistical analysis of the phosphorescence intensity in (b). Merged confocal image of living DC2.4 cell incubated with the WSP-CNDs @ silica excited at 405 nm, emission collected in the range of 415-500 (d) and 500-592 nm (e). (Scale bar, 50 μm).

fluorescence images and bight field images are shown in Fig. 4(d3), and they coincide each other well. In the range of 500−592 nm (Fig. 4(e2)), the DC2.4 cells showed intense green phosphorescence, which demonstrated that the WSP-CNDs @ silica can be rapidly and efficiently uptaken into DC2.4 cells and label the cells. Video S2 recorded luminescence processes of yeast cells incubated with WSP-CNDs @ silica aqueous solution. In a control group, the DC2.4 cells were pretreated with CNDs without phosphorescence for 2 h. No signals can be observed in the range of 500−592 nm, which indicates that the signals are from phosphorescence emission of the water-soluble phosphorescent CNDs (Fig. S22). These results indicated that the WSP-CNDs @ silica may be used for afterglow bioimaging.

The toxicity of the WSP-CNDs @ silica *in vivo* was studied and the bladder, brain, kidney, lung, spleen, liver, and heart of mice were collected to further evaluate whether they can eventually be applied in clinical research. The mice were treated with the WSP-CNDs @ silica *via* intravenous injection for 1 day and 7 days. The tissues were sliced and stained by hematoxylin and eosin (H&E), then carefully observed under the microscope to analyze if there were any pathological changes. From histological analysis results shown in Fig. 5(a), there is no symptom of inflammation or lesion in all tissues between the normal saline (control) and experimental groups.

The *in vivo* afterglow imaging was carried in an IVIS living imaging system by using the WSP-CNDs @ silica as afterglow agent, and the images were recorded under the bioluminescence mode. They was first irradiated with UV light for one minute to activate nanoparticles, and then the phosphorescence was collected after removal excitation source, as shown in Fig. 5(b). In Fig. 5(c), the phosphorescence of the WSP-CNDs @ silica can be easily detected after removal of excitation source and the phosphorescence intensity increases with increase their concentration . In order to evaluate their possibility for *in vivo* afterglow imaging, the WSP-CNDs @ silica were injected in subcutaneous of the dorsal area of mice. The WSP-CNDs @ silica were *in situ* illuminated for 1 min to active the phosphorescent CNDs, as shown in the left of Fig. 5(d). Subsequently, the images were taken in an IVIS living imaging system under the bioluminescence mode when the UV light source was removed, as shown in the right of Fig. 5(e). The phosphorescence signal of the WSP-CNDs @ silica can be easily detected, and the corresponding luminescence video is shown in

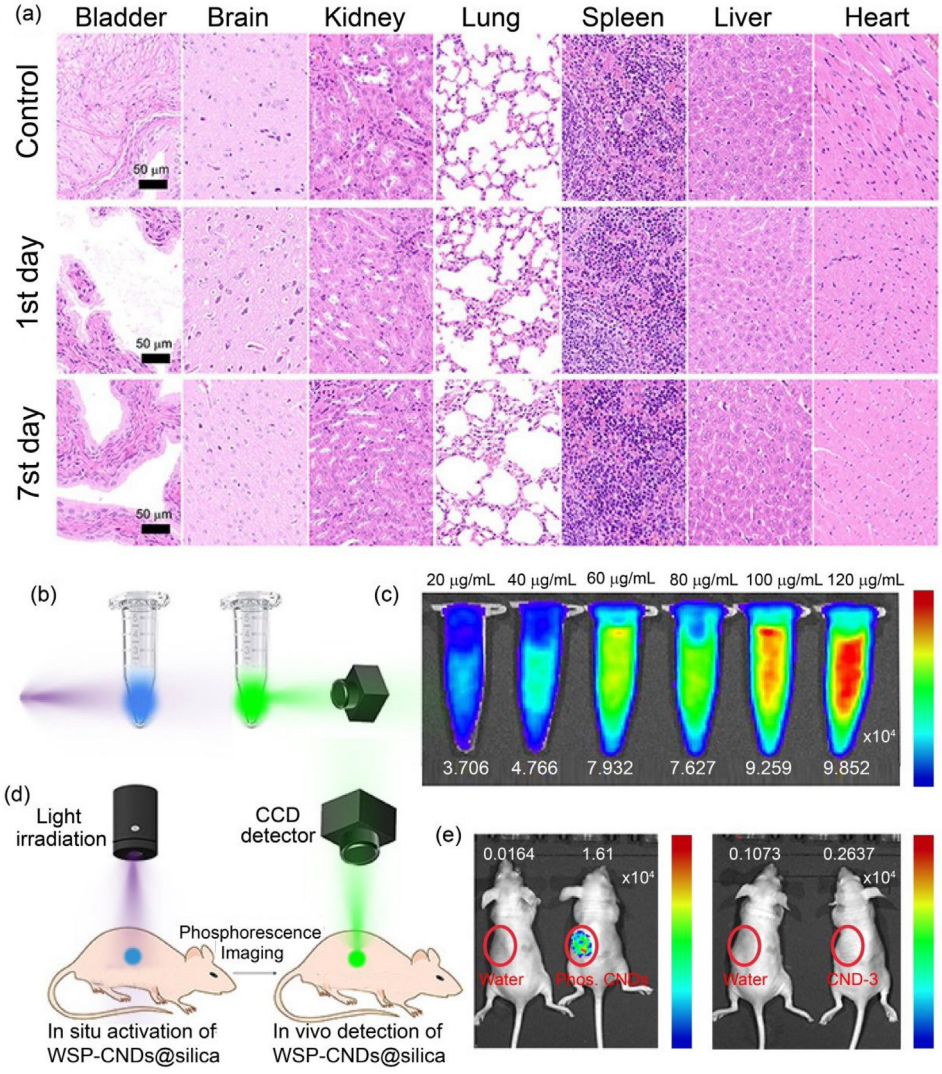

Fig. 5. (a) Hematoxylin and eosin stained slices of bladder, brain, kidney, lung, spleen, liver and heart tissues after the WSP-CNDs @ silica and control (normal saline) treatment. (Scale bar, 50 μm). (b) Schematic illustration of activation and detection of phosphorescence of the WSP-CNDs @ silica. (c) The phosphorescence images of the WSP-CNDs @ silica with different concentration. (d) Schematic illustration of *in situ* activation and detection of phosphorescence of the WSP-CNDs @ silica in living mice. (e) The phosphorescence imaging of two mice with the subcutaneous injection of the WSP-CNDs @ silica and water. The circles indicate the location of water and the WSP-CNDs @ silica.

Video S3. While it is hardly detectable under the same parameters for the fluorescent CNDs (control group). The above result indicates that the WSP-CNDs @ silica can be used as afterglow agent for afterglow bioimaging.

Conclusions

In summary, by confining the CNDs in a silica encapsulation layer to restrict the rotation and vibration of the bonds and isolate from oxygen molecules, phosphorescence has been realized from water-soluble CNDs. The lifetime and the phosphorescence QY of the phosphorescence can reach 1.86 s and 11.6 %, both of which are the best values ever reported for water-soluble phosphorescent nanoparticles. The water soluble phosphorescent CNDs present high stability and good biocompatibility, and afterglow bioimaging has been demonstrated by using the water soluble phosphorescent CNDs as afterglow agent. The results reported in this paper may push forward the application of phosphorescent nanoparticles in biomedical and clinic therapy, and may also expand the application of CNDs in afterglow bioimagings.

Methods

Materials

The precursors used in this study included ethylenediamine (EDA), purity > 99 %), phosphoric acid (purity > 95 %), and deionized water. All of the chemicals were purchased from Macklin Chemistry Co. Ltd (Shanghai, China). Note that all the chemicals used in this work were analytical grade without further purification.

Synthesis of CNDs

1.0 mL of EDA was firstly dissolved in 15 mL deionized water, and then 2 mL of phosphoric acid was slowly added into the EDA aqueous solution with stirring for 30 min. The formed transparent solution was then heated in a microwave oven (750 W) for 110 s (CND-1), 120 s (CND-2) and 130 s (CND-3). When the samples cooled down to room temperature, 20 mL deionized water was added into above samples and the light yellow solution was formed. The aqueous solution was centrifuged for 10 min in order to remove sediment. The supernatant was filtered through 0.22 μm membrane and then neutralized by sodium carbonate. The supernatant was collected and subjected to dialysis (MWCO: 500 Da) for a week. Finally, pale yellow solid CND powder was obtained by freeze-drying.

Synthesis of the WSP-CNDs @ silica

1 mL CND-3 (100 μg/mL) aqueous solution and 0.5 mL tetraethoxysilane (TEOs) were dispersed in 15 mL deionized water to form aqueous solution. Then, 0.5 mL ammonia was placed into the above solution stirring at room temperature for 8 h. The transparent solution was collected and filtered through 0.22 μm membrane for several times. Finally, transparent solution was obtained.

Phosphorescence quantum yield measurement

The phosphorescence quantum yield (QY) of the WSP-CNDs @ silica was measured by a FLS980 spectrometer with a calibrated integrating sphere in. In principle, the phosphorescence QY can be expressed by the following equation:

$$\eta = \frac{\varepsilon}{\alpha} = \frac{\int_{390}^{750} L_{emission}}{\int E_{reference} - \int \mathrm{E}_{\mathrm{sample}}} = \frac{number\ of\ emitted\ photons}{number\ of\ absorbed\ photons}$$

where η is total luminescence QY, ε is the emitted photons of the sample that collected by the integrating sphere in the range of 390−770 nm, α is the photons absorbed by the sample. L_{emission} is the net emission of the sample. $E_{\mathrm{reference}}$ is the absorption spectrum of the reference in the sphere. E_{sample} is the absorption spectrum of the sample and reference. The calculated luminescence QY of WSP-CNDs @ silica in the range of 390−770 nm is about 25.21 % based on above equation. The proportion of phosphorescence is about 46 % in the total luminescence intensity, thus the phosphorescence QY is about 11.6 %

Temporal stability test

The WSP-CNDs @ silica solution was stored in a glass bottle at room temperature (25 °C). The phosphorescence spectra of the WSP-CNDs @ silica were collected at interval of five days for 40 days. At the same time, the phosphorescence images of the WSP-CNDs @ silica were taken under condition of sunlight and UV off, respectively.

Photostability test

The WSP-CNDs @ silica were continuously irradiated by a UV light (0.15 mW/cm^{-2}) and the phosphorescence spectra of the WSP-CNDs @ silica were collected at interval of 5 min for 35 min.

Cycle test

The phosphorescence spectra of the WSP-CNDs @ silica were collected under the condition of UV on/off for several cycles, and peaks intensity of the corresponding spectra were plotted *versus* cycle number.

Cellular toxicity test

CHO-K1 cells (1000 cells/200 μL) were cultured in 96-well plates for 24, 48 and 72 h in an incubator (37 °C, 5% CO_2). Then, the culture medium was replaced by fresh medium, which contained the water-soluble phosphorescent CNDs with different concentrations (0, 12.5, 25, 50 and 100 μg/mL). MTT solution was added to each well. The microplate reader was used to monitor absorbance at 490 nm. The cell viability was evaluated according to the following equation:

$$\mathrm{CellViability}(\%) = \mathrm{OD}_{\mathrm{Treated}}/\mathrm{OD}_{\mathrm{Control}}$$

Flow cytometry analysis

DC2.4 cells (5 × 105) were incubated with 20 μg CDs or phosphate buffer saline (control) for 2 h at 37 °C, then cells were washed once with phosphate buffer saline. The DC2.4 cells were pre-irradiated by 365 nm laser for 1 min, and then the afterglow phosphorescent were detected by a flow cytometry.

Cellular imaging

For cellular imaging, DC2.4 cells were incubated with the water-soluble phosphorescent CNDs (100 μg/mL) in an incubator (37 °C, 5% CO_2) for 2 h. Then the cells were fixed on the slide. Prior to fixation of the cells on the slide for inspection with a fluorescence

microscope, the excess water-soluble phosphorescent CNDs were removed by washing 3 times with PBS buffer. Cells loaded with the water-soluble phosphorescent CNDs were excited at 405 nm and the signal was collected in the range from 408 to 500 nm and from 500 nm to 592 nm.

Histological analysis

Mice were treated with 100 μg CNDs for 1 day and 7 days *via* intravenous injection. At the same time, the control mice were treated with normal saline. Then mice were sacrificed and harvested heart, kidney, bladder, liver, lung, brain and spleen. The principle organs were excised and immediately fixed in neutral fixative for histopathological examination.

Mice

Female BALB/c and BALB/c nude mice, aged 6–8 weeks, were purchased from Vital River Laboratory Animal Technology Co. Ltd (Beijing, China). All mice maintained in a specific pathogen-free facility. Animal welfare and experimental procedures were carried out in accordance with national and institutional guidelines for animal care and were approved by the Ethics Committee of Zhengzhou University.

Fluorescence and afterglow bioimaging

Female BALB/c nude mice were used for *in vivo* subcutaneous imaging. The mice were anesthetized using isoflurane and the water-soluble phosphorescent CNDs solution was injected into the dorsal areas of mice (100 μg/mL). Before the living imaging, the water-soluble phosphorescent CNDs were activated by hand held UV lamp for 1 min. The signals were collected after removal exciting source using IVIS living imaging system under the bioluminescence mode.

Characterization

TEM images were recorded on JSM-6700 F. PL and phosphorescence spectra were performed on obtained on Hitachi F-7000 spectrophotometer. The lifetimes of the CNDs were measured by time correlated single photon counting on a FLS980 spectrometer with excitation of 350 nm at room temperature. Time-resolved emission spectra and kinetic measurements were recorded by OmniFluo990 (Zolix Instruments Co., Ltd., China). X-ray diffraction (XRD) patterns were obtained on X'Pert Pro diffractometer. Fourier transform infrared (FTIR) spectra were obtained on a Nicolet 6700 spectrometer (Thermo Fisher Scientific, USA). The X-ray photoelectron spectra (XPS) were obtained using PERKIN ELMZR PHI 3056. Raman spectra were measured on a Horiba-HR-800 Raman spectroscopy system.

Author contributions

K.L. conceived the idea; C. Shan and K. Liu supervised and coordinated all aspects of the project. Y. Liang carried out synthesis and characterization, Y. Liang and K. Liu wrote the paper. S. G. did biological experiments. W.W., Q.L., X.W., J.Z., Y. G and L.D. commented the paper and all authors discussed the results.

Declaration of Competing Interest

There are no conflicts of interest

Acknowledgment

Y. Liang and S. Gou contributed equally to this work. This work was supported by the National Natural Science Foundation of China (Grant Nos. 11904326, U1804155, and U1604263), China Postdoctoral Science Foundation (2019TQ0287, 2019M662510).

Appendix A. Supplementary data

Supplementary material related to this article can be found, in the online version, at doi:https://doi.org/10.1016/j.nantod.2020.100900.

References

[1] Y. Fan, P. Wang, Y. Lu, R. Wang, L. Zhou, X. Zheng, X. Li, J. Piper, F. Zhang, Nat. Nanotechnol. 13 (2018) 941, http://dx.doi.org/10.1038/s41565-018-0221-0.
[2] C. Sun, B. Li, M. Zhao, S. Wang, Z. Lei, L. Lu, H. Zhang, L. Feng, C. Dou, D. Yin, H. Xu, Y. Cheng, F. Zhang, J. Am. Chem. Soc. 141 (2019) 19221, http://dx.doi.org/10.1021/jacs.9b10043.
[3] Y. Fan, S. Wang, F. Zhang, Angew. Chem., Int. Ed. 16 (2019) 13208, http://dx.doi.org/10.1002/anie.201901964.
[4] L. Xiao, Z. Chen, B. Qu, J. Luo, S. Kong, Q. Gong, J. Kido, Adv. Mater 23 (2011) 926, http://dx.doi.org/10.1002/adma.201003128.
[5] X. Zhen, Y. Tao, Z. An, P. Chen, C. Xu, R. Chen, W. Huang, K. Pu,Adv. Mater. 29 (2017), 1606665, http://dx.doi.org/10.1002/adma.201606665.
[6] S. Cai, H. Shi, J. Li, L. Gu, Y. Ni, Z. Cheng, S. Wang, W. Xiong, L. Li, Z. An, W. Huang,Adv. Mater. 29 (2017), 1701244, http://dx.doi.org/10.1002/adma.201701244.
[7] L. Hu, P. Wang, M. Zhao, L. Liu, L. Zhou, B. Li, F. Albaqami, A. El-Toni, X. Li, Y. Xie, X. Sun, F. Zhang, Biomaterials 163 (2018) 154, http://dx.doi.org/10.1016/j.biomaterials.2018.02.029.
[8] L. Hu, Y. Fan, L. Liu, X. Li, B. Zhao, R. Wang, P. Wang, A.M.E. Toni, Adv. Fan Zhang,Opt. Mater. Express 5 (2017), 1700680, http://dx.doi.org/10.1002/adom.201700680.
[9] H. Zhang, Y. Fan, P. Pei, C. Sun, L. Lu, F. Zhang, Angew. Chem., Int. Ed. 58 (2019) 10153, http://dx.doi.org/10.1002/anie.201903536.
[10] S. Tao, S. Lu, Y. Geng, S. Zhu, S.A.T. Redfern, Y. Song, T. Feng, W. Xu, B. Yang, Angew. Chem., Int. Ed. 57 (2018) 2393, http://dx.doi.org/10.1002/anie.201712662.
[11] Q. Li, M. Zhou, Q. Yang, Q. Wu, J. Shi, A. Gong, M. Yang, Chem. Mater. 28 (2016) 8221, https://doi.org/0.1021/acs.langmuir.8b00939.
[12] K. Jiang, Y. Wang, X. Gao, C. Cai, H. Lin, Angew. Chem., Int. Ed. 57 (2018) 6216, http://dx.doi.org/10.1002/anie.201802441.
[13] C. Xia, S. Tao, S. Zhu, Y. Song, T. Feng, Q. Zeng, J. Liu, B. Yang, Chem. Eur. J. 24 (2018) 11303, http://dx.doi.org/10.1002/chem.201802712.
[14] J. Liu, N. Wang, Y. Yu, Y. Yan, H. Zhang, J. Li, J. Yu,Sci. Adv. 3 (2017), e1603171, http://dx.doi.org/10.1002/adma.201003128.
[15] K. Jiang, L. Zhang, J. Lu, C. Xu, C. Cai, H. Lin, Angew. Chem., Int. Ed. 55 (2016) 7231, http://dx.doi.org/10.1002/anie.201602445.
[16] C. Lin, Y. Zhuang, W. Li, T. Zhou, R. Xie, Nanoscale 11 (2019) 6584, http://dx.doi.org/10.1039/c8nr09672d.
[17] J. Li, B. Wang, H. Zhang, J. Yu,Small 15 (2019), 1805504, http://dx.doi.org/10.1002/smll.201805504.
[18] L. Bian, H. Shi, X. Wang, K. Ling, H. Ma, M. Li, Z. Cheng, C. Ma, S. Cai, Q. Wu, N. Gan, X. Xu, Z. An, W. Huang, J. Am. Chem. Soc. 140 (2018) 10734, http://dx.doi.org/10.1021/jacs.8b03867.
[19] H. Chen, X. Yao, X. Ma, H. Tian, Adv. Opt. Mater. 4 (2018) 1397, http://dx.doi.org/10.1002/adom.201600427.
[20] S.M.A. Fateminia, Z. Mao, S. Xu, Z. Yang, Z. Chi, B. Liu, Angew. Chem., Int. Ed. 56 (2018) 12160, http://dx.doi.org/10.1002/anie.201705945.
[21] S. Pan, Z. Chen, X. Zheng, D. Wu, G. Chen, J. Xu, H. Feng, Z. Qian, J. Phys. Chem. Lett. 9 (2018) 3939, http://dx.doi.org/10.1021/acs.jpclett.8b01697.
[22] Z. An, C. Zheng, Y. Tao, R. Chen, H. Shi, T. Chen, Z. Wang, H. Li, R. Deng, X. Liu, W. Huang, Nat. Mater. 14 (2015) 685, http://dx.doi.org/10.1038/nmat4259.
[23] Z. Chen, Z. Bian, C. Huang, Adv. Mater. 22 (2010) 1534, http://dx.doi.org/10.1002/adma.200903233.
[24] D.G. Cuttell, S. Kuang, P.E. Fanwick, D.R. McMillin, R.A. Walton, J. Am. Chem. Soc. 124 (2002) 6, http://dx.doi.org/10.1021/ja012247h.
[25] A. Abdukayum, J. Chen, Q. Zhao, X. Yan, J. Am. Chem. Soc. 135 (2013) 14125, http://dx.doi.org/10.1021/ja404243v.
[26] K.K. Liu, S.Y. Song, L.Z. Sui, S.X. Wu, P.T. Jing, R.Q. Wang, Q.Y. Li, G.R. Wu, Z.Z. Zhang, K.J. Yuan, C.X. Shan,Adv. Sci. 6 (2019), 1900766, http://dx.doi.org/10.1002/advs.201900766.
[27] S. Song, K. Liu, J. Wei, Q. Lou, Y. Shang, C. Shan, Nano Lett. 19 (2019) 5553, http://dx.doi.org/10.1021/acs.nanolett.9b02093.
[28] J. Zhu, X. Bai, X. Chen, H. Shao, Y. Zhai, G. Pan, H. Zhang, E.V. Ushakova, Y. Zhang, H. Song, A.L. Rogach,Adv. Optical Mater. 7 (2019), 1801599, http://dx.doi.org/10.1002/adom.201801599.
[29] K. Hola, Y. Zhang, Y. Wang, E.P. Giannelis, R. Zboril, A.L. Rogach, Nano Today 9 (2014) 590, http://dx.doi.org/10.1016/j.nantod.2014.09.004.

[30] Z. Wang, F. Yuan, X. Li, Y. Li, H. Zhong, L. Fan, S. Yang,Adv. Mater. 29 (2017), 1702910, http://dx.doi.org/10.1002/adma.201702910.
[31] T. Feng, Q. Zeng, S. Lu, X. Yan, J. Liu, S. Tao, M. Yang, B. Yang, ACS Photonics 5 (2017) 502, http://dx.doi.org/10.1021/acsphotonics.7b01010.
[32] M. Han, S.J. Zhu, S.Y. Lu, Y.B. Song, T.L. Feng, S.Y. Tao, J.J. Liu, B. Yang, Nano Today 19 (2018) 201, http://dx.doi.org/10.1016/j.nantod.2018.02.008.
[33] X. Li, Y. Liu, X. Song, H. Wang, H. Gu, H. Zeng, Angew. Chem., Int. Ed. 54 (2015) 1759, http://dx.doi.org/10.1002/ange.201406836.
[34] W. Chen, D. Li, L. Tian, W. Xiang, T. Wang, W. Hu, Y. Hu, S. Chen, J. Chen, Z. Dai, Green Chem. 20 (2018) 4438, http://dx.doi.org/10.1039/c8gc02106f.
[35] C. Shen, Q. Lou, J. Zang, K. Liu, S. Qu, L. Dong, C. Shan, Adv. Sci. (2020) 1903525, http://dx.doi.org/10.1002/advs.201903525.
[36] D. Qu, M. Zheng, J. Li, Z. Xie, Z. Sun, Light Sci. Appl. 4 (2015) e364, http://dx.doi.org/10.1038/lsa.2015.137.
[37] X. Bao, E.V. Ushakova, E. Liu, Z. Zhou, D. Li, D. Zhou, S. Qu, A.L. Rogach, Nanoscale 11 (2019) 14250, http://dx.doi.org/10.1039/c9nr05123f.
[38] X. Dong, L. Wei, Y. Su, Z. Li, H. Geng, C. Yang, Y. Zhang, J. Mater. Chem. C 3 (2015) 2798, http://dx.doi.org/10.1039/c5tc00126a.
[39] H. Mieno, R. Kabe, N. Notsuka, M.D. Allendorf, C. Adachi, Adv. Opt. Mater. 4 (2016) 1015, http://dx.doi.org/10.1002/adom.201600103.
[40] K. Jiang, Y. Wang, C. Cai, H. Lin, Chem. Mater. 29 (2017) 4866, http://dx.doi.org/10.1021/acs.chemmater.7b00831.
[41] Q. Li, M. Zhou, M. Yang, Q. Yang, Z. Zhang, J. Shi, Nat. Commun. 9 (2018) 734, http://dx.doi.org/10.1038/s41467-018-03144-9.
[42] Y. Gao, H. Zhang, Y. Jiao, W. Lu, Y. Liu, H. Han, X. Gong, S. Shuang, Chem. Mater. 31 (2019) 7979, http://dx.doi.org/10.1021/acs.chemmater.9b02176.
[43] L. Wei, S. Wu, X. Xu, J. Zhuang, H. Zhang, X. Zhang, C. Hu, B. Lei, Clemens F. Kaminski, Y. Liu, Chem. Mater. 31 (2019) 9887, http://dx.doi.org/10.1021/acs.chemmater.9b04120.
[44] Y. Liang, Y. Shang, K. Liu, Z. Liu, W. Wu, Q. Liu, Q. Zhao, X. Wu, L. Dong, C. Shan, Nano Res. (2020), http://dx.doi.org/10.1007/s12274-020-2710-3.
[45] K. Liu, Q. Liu, D. Yang, Y. Liang, L. Sui, J. Wei, G. Xue, W. Zhao, X. Wu, L. Dong, C. Shan, Light Sci. Appl. 9 (2020) 44, http://dx.doi.org/10.1038/s41377-020-0283-2.
[46] D. Zhou, D. Li, P. Jing, Y. Zhai, D. Shen, S. Qu, A.L. Rogach, Chem. Mater. 29 (2017) 1779, http://dx.doi.org/10.1021/acs.chemmater.6b05375.
[47] S.M. Ali Fateminia, Z. Mao, S.D. Xu, Z.Y. Yang, Z.G. Chi, B. Liu, Angew. Chem. Int. Ed. 56 (2017) 12160, http://dx.doi.org/10.1002/anie.201705945.
[48] H. Zhang, H. Gao, S. Zhang, S. Zhang, S. Zheng, Y. Wang, Z. Zhao, D. Ding, B. Yang, Y. Zhang, W. Yuan,Adv. Mater. 31 (2019), 1807222, http://dx.doi.org/10.1002/adma.201807222.

Ya-Chuan Liang obtained his Master's degree in condensed matter physics from Zhengzhou University in 2018. Currently, he is a Ph.D. student under the supervision of Prof. Chongxin Shan at Zhengzhou University. His research interests focused on luminescent carbon-based nanomaterials for biomedical applications.

Shan-Shan Gou obtained her bachelor degree in biological science from Xinyang Normal University in 2016. Currently, she is a Ph.D. student in the lab of Prof. Yanfeng Gao at Zhengzhou University. Her main research interests focus on dendritic cell-based cancer vaccine.

Dr. Kai-Kai Liu received his BS in Applied Physics from Shandong University (2013) and Ph. D. in Condensed Matter Physics from Changchun Institute of Optics, Fine Mechanics and Physics, Chinese Academy of Sciences (2018). Since 2018, he worked at School of Physics and Microelectronics, Zhengzhou University. Currently, his research focused on luminescent nanomaterials, including carbon-based nanodots, ZnO quantum dots and perovskite quantum dots.

Wen-Jie Wu obtained her BS degree in physics in Zhoukou Normal University in 2018. She is now a master student under the supervision of Ph.D. Qi Zhao at Zhengzhou University. Her research interests focused on the synthesis and optoelectronic applications of ZnO.

Chen-Zi Guo is a PhD student in Changchun Institute of Optics, Fine Mechanics and Physics, Chinese Academy of Sciences. She received her bachelor and master degree in Harbin Institute of Technology and she serves as an Editor of *Light: Science & Applications*

Si-Yu Lu is currently an associate professor of College of Chemistry, Zhengzhou University. He received his Ph.D. degree in polymer physics and chemistry under the supervision of Prof. Bai Yang at Jilin University. His research interests relate to the design, preparation, properties of photoelectric nanocrystals (Carbon dots, Semiconductors, *etc.*) and their applications in catalysis, fluorescence and DFT calculation

Jin-Hao Zang received his MS degree from Northwest Univeristy in 2008. He is currently an experimentalist in School of Physics at Zhengzhou University. His research focuses on high pressure synthesis of novel materials.

Xue-Ying Wu obtained his BS degree in physics in Zhengzhou Normal University in 2017. She is now a master student under the supervision of Ph.D. Qi Zhao at Zhengzhou University. Her research interests focused on the synthesis and optoelectronic applications of nanodiamond and ZnO.

Qing Lou, graduated in 2012 at Chongqing University and earned his PhD in Condensed Matter Physics (2015) at the Changchun Institute of Optics, Fine Mechanics and Physics (CIOMP), Chinese Academy of Sciences. In 2015, he entered into Zhengzhou University as a lecturer in the Diamond Optoelectronic Materials and Devices Group directed by Prof. Chong-Xin Shan. His research revolves around carbon materials (diamond and carbon quantum dot) and related optoelectronic devices.

Prof. Lin Dong received his B.S. (1998) and M.S. degree (2001) in Chemistry from Jilin University, and the Ph.D. degree (2005) in Condensed Matter Physics from Changchun Institute of Optics, Fine Mechanics and Physics, CAS, and joined Zhengzhou University in 2005. He visited at Georgia Institute of Technology during 2011~2012, and Beijing Institute of Nanoenergy and Nanosystem during 2012~2015 as the visiting professor. He is currently a full professor in School of Physics & Microelectronics, Zhengzhou University. His research mainly focuses on luminescent performance and piezotronic/piezophototronic effects of nano-devices. http://www.researcherid.com/rid/A-1499-2012

Dr. Yan-Feng Gao is a Professor of Medicine at Zhengzhou University. He got the doctoral degree at Lanzhou University in 2006. His main research interests include cancer immunotherapy, medicinal chemistry and nanomedicine.

Chong-Xin Shan is a Professor of Zhengzhou University. He received his BS degree from Wuhan University in 1999, and PhD degree from Changchun Institute of Optics, Fine Mechanics and Physics, Chinese Academy of Sciences in 2004. His current research focused on semiconductor optoelectronic materials and devices. He has been supported by National Science Fund for Distinguished Young Scholars, Distinguished professor of Changjiang Scholars, *etc.*